Lab on a Chip

Miniaturisation for chemistry, physics, biology, materials science and bioengineering

www.rsc.org/loc

Volume 11 | Number 21 | 7 November 2011 | Pages 3567–3726

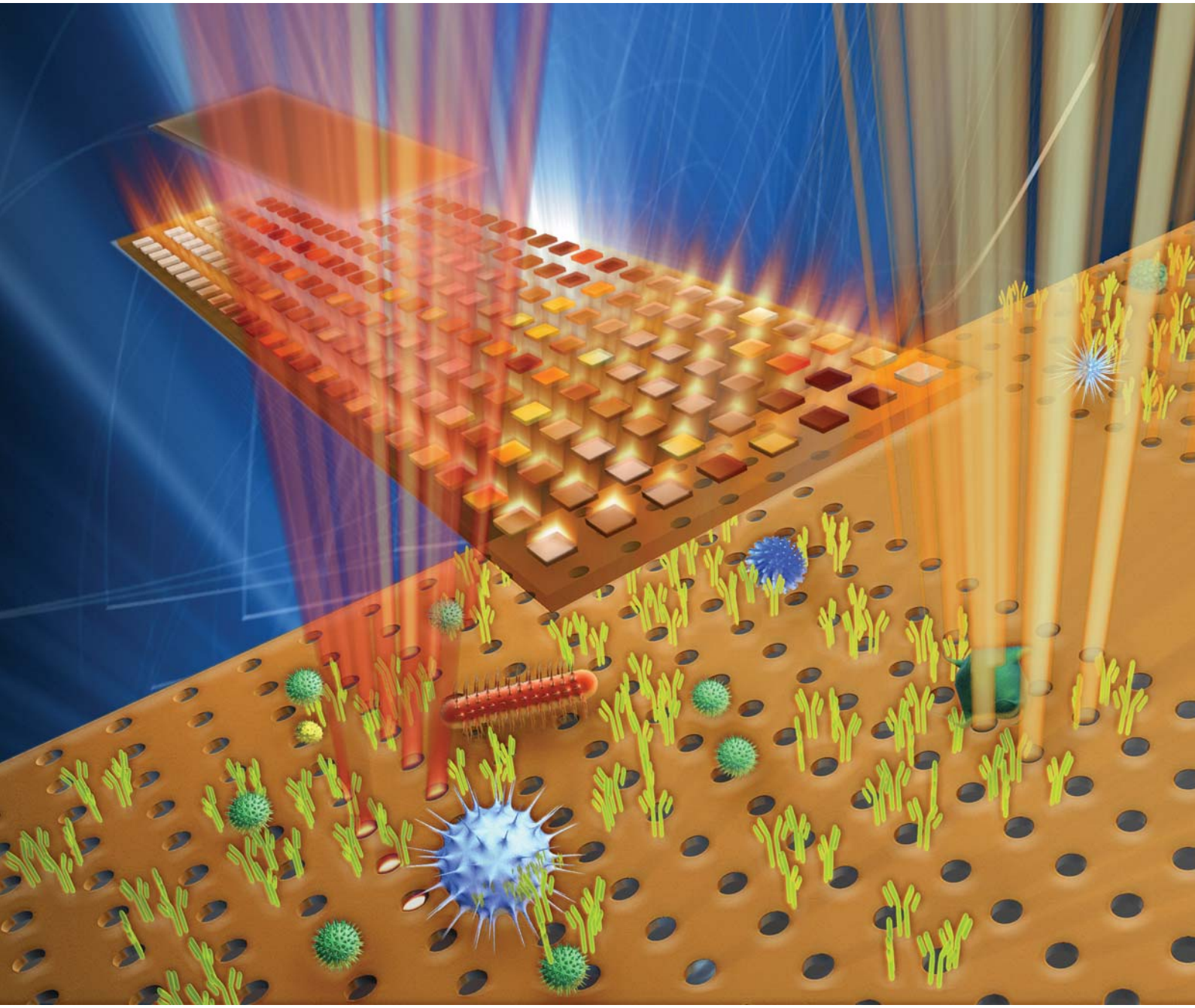

ISSN 1473-0197

RSC Publishing

PAPER

Hatice Altug *et al.*

Large-scale plasmonic microarrays for label-free high-throughput screening

1473-0197(2011)11:21;1-2

Lab on a Chip

Dynamic Article Links

Cite this: *Lab Chip*, 2011, **11**, 3596

www.rsc.org/loc

PAPER

Large-scale plasmonic microarrays for label-free high-throughput screening†

Tsung-Yao Chang,‡[a] Min Huang,‡[b] Ahmet Ali Yanik,[b] Hsin-Yu Tsai,[a] Peng Shi,[a] Serap Aksu,[b] Mehmet Fatih Yanik*[ac] and Hatice Altug*[b]

Received 1st June 2011, Accepted 9th August 2011
DOI: 10.1039/c1lc20475k

Microarrays allowing simultaneous analysis of thousands of parameters can significantly accelerate screening of large libraries of pharmaceutical compounds and biomolecular interactions. For large-scale studies on diverse biomedical samples, reliable, label-free, and high-content microarrays are needed. In this work, using large-area plasmonic nanohole arrays, we demonstrate for the first time a large-scale label-free microarray technology with over one million sensors on a single microscope slide. A dual-color filter imaging method is introduced to dramatically increase the accuracy, reliability, and signal-to-noise ratio of the sensors in a highly multiplexed manner. We used our technology to quantitatively measure protein-protein interactions. Our platform, which is highly compatible with the current microarray scanning systems can enable a powerful screening technology and facilitate diagnosis and treatment of diseases.

High-throughput functional study of proteins is important for early detection of diseases as well as for discovery of drug targets. Microarray analysis of proteins, nucleic acids, and chemicals provides an approach to efficiently identify protein–protein interactions, transcription profiles, and small molecule drug candidates.[1–4] Current microarray technologies rely on label-based fluorescence detection. However, labels often sterically interfere with molecular binding interactions and lead to inaccurate measurements.[5,6] Photo-bleaching and quenching of labels also cause further limitations for real-time and quantitative analysis of biomolecular interactions.[7] Moreover, fluorescence-labeling on a large number of proteins is costly and time-consuming. Therefore, there is a significant need for label-free, large-scale, quantitative and high-throughput detection systems that can reliably and sensitively identify biomolecular interactions.

In the last decade, electrical,[8,9] mechanical[10–12] and optical[13–19] sensing techniques have been proposed for label-free multiplexing applications. Among these, photonics-based approaches are highly advantageous. Optical biosensors allow transduction of the biomolecular binding signal remotely from the sensing volume, thereby minimizing sample contamination. Unlike mechanical and electrical sensors, they are also compatible with physiological solutions and are not sensitive to changes in the ionic strengths of the analyte solutions. Among optical sensors, methods exploiting surface plasmon resonance (SPR) are taking the lead. Surface plasmons, electromagnetic excitations propagating at metal/dielectric interfaces associated with the collective oscillations of electrons, can interrogate minute changes within the close vicinity of the interface. In fact, SPR is considered as the gold standard technique for label free-detection.[20] Although SPR sensors have relatively high sensitivity, their large-scale multiplexing has been severely limited due to the need for an alignment sensitive prism coupling scheme that requires bulky instrumentation.[21]

Recently, sub-wavelength plasmonic nanohole arrays have generated much interest for label-free biosensing due to their potential for high-throughput multiplexing.[22–26] Nanohole arrays enable extraordinary optical transmission (EOT) through thick metal films by direct coupling of perpendicularly incident light to the plasmonic excitations.[27–30] The resonance wavelength of EOT signal is strongly dependent on the effective dielectric constant of the adjacent medium around the nanohole arrays and can be used to detect any binding process without the use of labels.[31,32] A collinear excitation/collection coupling scheme combined with the small footprint of sensors provide unique opportunities to realize large-scale microarrays that can perform studies with minute amounts of biological samples. This is highly advantageous compared to high-quality factor dielectric microcavities, including photonic crystals[33,34] and whispery gallery mode resonators[35] suffering from alignment sensitive coupling schemes. As shown in Fig. 1, the transmitted EOT signal from each sensor can be directly imaged onto a charge-coupled device (CCD). The change in medium around the individual nanohole array sensor, before and after the binding events, can be detected by

[a]*Department of Electrical Engineering and Computer Science, Massachusetts Institute of Technology, Cambridge, Massachusetts, 02139, USA. E-mail: yanik@mit.edu*
[b]*Department of Electrical and Computer Engineering, Boston University, Boston, 02215, USA. E-mail: altug@bu.edu*
[c]*Department of Biological Engineering, Massachusetts Institute of Technology, Cambridge, 02139, USA*

† Competing interest statement: The authors declare that they have no competing financial interest.

‡ These authors contributed equally to this work.

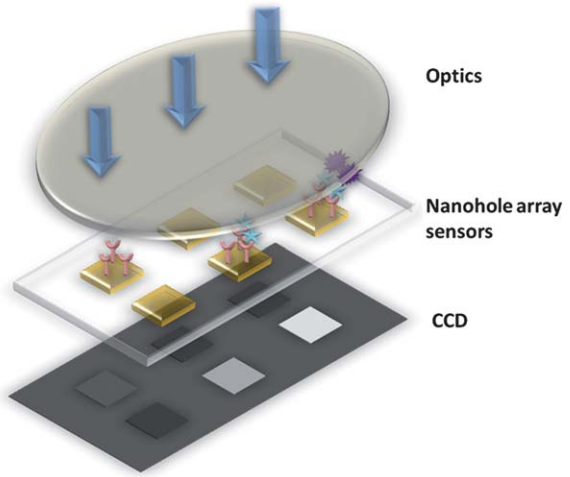

Fig. 1 Scheme of plasmonic nanohole arrays as biochemical sensors. Collimated light transmits through plasmonic nanohole array sensors and gets imaged by the CCD camera. Intensities shown on the CCD camera can be used to analyze the molecule accumulations on the sensor pixels in a high-throughput fashion.

monitoring the intensity modulation at the corresponding CCD pixels. However, current measurements[31,36] based on intensity variations at a single wavelength have been significantly unreliable and restrictive for multiplexing due to the intensity fluctuations caused by molecular absorptions as well as amplitude noises. Alternative detection techniques are necessary for rapid, highly reliable and large-scale microarray sensing. Also, it is crucial to introduce low-cost nanofabrication techniques for wide adaptation of nano-biochemical sensors.[37]

In this paper, we demonstrate a high-density label-free biodetection platform for reliable and massively multiplexed detection of biomolecular bindings. To achieve this, we introduce a dual-color filter imaging method (DcFI). This method allows identification of spectral shifts reproducibly in a multiplexed manner with more than 30 times improved signal-to-noise ratios (SNR) compared to methods based on direct intensity changes. Our method also reduces image acquisition time with respect to fluorescence techniques by two orders of magnitude. To create large-scale microarrays, we use interference lithography to fabricate 1.5 million sensors on a single microscope slide with a packing density of nearly one thousand sensors per mm^2. High optical quality of the fabricated devices is confirmed with refractive index-based measurements showing high sensitivities[22] around 615 nm/RIU (RIU stands for refractive index unit). Sharp plasmonic resonances with line-widths as narrow as 22.5 nm full-width-at-half-maximum (FWHM) are observed. Using this platform, we demonstrate quantitative measurements of antibody bindings at a variety of concentrations in a label-free fashion.

Results

Fabrication of plasmonic microarray

Large-scale and cost-effective patterning of nanohole arrays on a regular microscope glass slide is achieved using interference lithography technique as shown in Fig. 2a. Then, arrays of microscale sensing pixels are formed upon these nanoholes *via* photolithography and chromium deposition. Further detail of nanofabrication process is discussed in Method section. These sensing pixels are identical 20 μm by 20 μm squares and separated by 15 μm from each other. The size of a standard microscope glass slide is 75 mm by 25 mm. As a result, up to 1.5 million sensor pixels have been fabricated on a single glass substrate with a packing density of 816 sensors per mm^2. The number of sensor elements on this plasmonic microarray is comparable to that of state-of-the-art fluorescence based microarrays. Such a dense multiplexing capability is sufficient for screening large-scale protein libraries containing 30,000∼40,000 types of proteins. Scanning electron microscope (SEM) images of the fabricated microarrays are shown in Fig. 2b-2e. Fig. 2b shows the large-scale view of the microarray. Each individual sensor contains around 33 by 33 nanoholes. High uniformity and structural quality of the gold nanohole structures (Fig. 2c and Fig. 2d) confirm the robustness of the interference lithography technique. Moreover, the tilted (30°) SEM image in Fig. 2e shows straight sidewalls. The periodicity of the nanohole arrays shown in the SEM images is 600 nm and the diameter of nanoholes is 200 nm.

Optical performance of the microarray

To experimentally evaluate the optical response of the nanohole arrays, transmission spectra were obtained using a collimated broadband light source at normal incidence. The transmitted signal was collected by an objective lens with 100x magnification and 0.7 numerical aperture, and fiber-coupled to a spectrometer. Fig. 3 shows the transmission spectrum of 200 nm radius Au nanohole array with 600 nm periodicity. The comparison between the finite-difference time-domain simulation (black) and experimental (red dashed) results in air shows good agreement for the (1,0) Au-air interface resonance. The (1,0) resonance wavelength red-shifts with increasing refractive index of the solution (water, acetone and isopropyl alcohol (IPA)). The sensitivity reaches up to 615 nm/RIU, which is comparable to the high value we previously demonstrated[21] with suspended nanohole arrays fabricated by electron beam lithography. To evaluate intrinsic detection limits of optical nanoscale sensors, literature commonly uses figure of merit (FOM), which is defined as the sensitivity divided by the FWHM of a Lorentzian shaped resonance. In this work, experimentally obtained FOMs are 27 for the (1,0) resonances over the entire microarray. Inset in Fig. 3 shows the transmission signal captured by the CCD camera. Light intensities coming from different sensor pixels are very uniform over the microscope slide. These results confirm that sensor devices with high optical quality can be fabricated uniformly over large areas by using interference lithography.

To functionalize microscale sensors with specific biomolecules, we utilized a high precision biomolecule spotting technique based on dip-pen lithography (BioForce Nanosciences TM). This capability is confirmed with spotted fluorescent antibodies on protein A/G functionalized sensors. Anti-mouse immunoglobulin (IgG) from goat (labeled with TRITC, red) and anti-monkey IgG from rabbit (labeled with FITC, green), are spotted onto the sensors. Fig. 4a shows the fluorescence signal from the spotted area. The spots are well defined and separated, and the individual

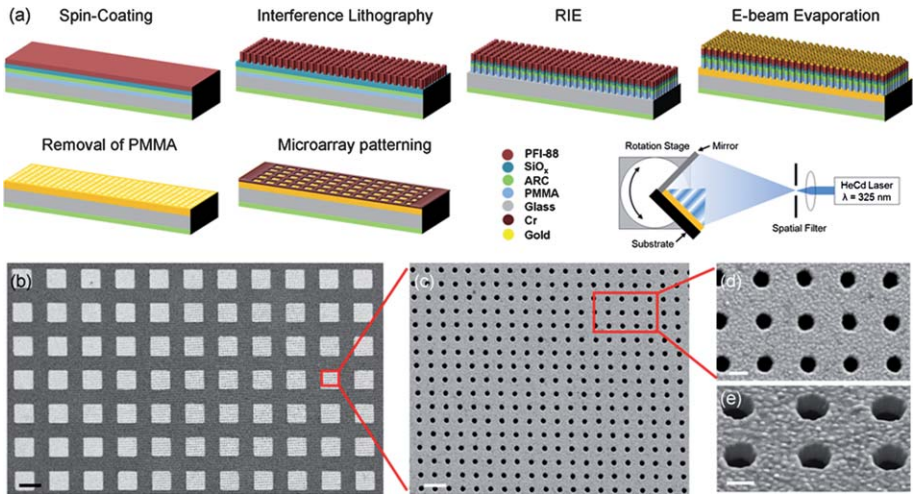

Fig. 2 Microarray fabrication scheme and SEM images. **(a)** Schematic representation of the fabrication process. Sensing pixel arrays are patterned on a standard microscope glass slide (75 mm by 25 mm) using interference lithography technique. **(b)** SEM images of the microarray with 7 by 11 sensor elements. Scale bar, 20 μm. **(c)** Top view image of the part of a sensor pixel. Scale bar, 1 μm. **(d)** Further enlarged image shows the uniformity and roundness of the nanohole arrays. Scale bar, 250 nm. **(e)** 30° tilted view reveals the verticality of edges. Scale bar, 200 nm.

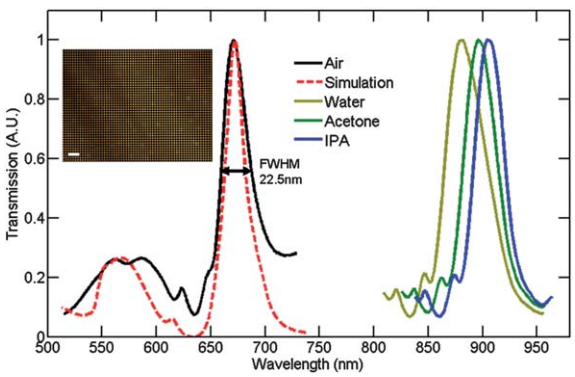

Fig. 3 Transmission spectra of the nanohole arrays and its sensitivity to the surrounding refractive index changes. Experimental (black) and finite-difference time-domain simulation (red dashed line) spectra match well over the spectral region of interest. The surface plasmon resonance peak is due to resonance at the Au-air interface. Spectral shifts as the refractive index of the solution changes show high sensitivity (615 nm/RIU) of the nanoholes with narrow resonances (FWHM = 22.5 nm). The experimentally obtained figure of merit is 27. Inset shows the image of the microarray. Scale bar, 50 μm.

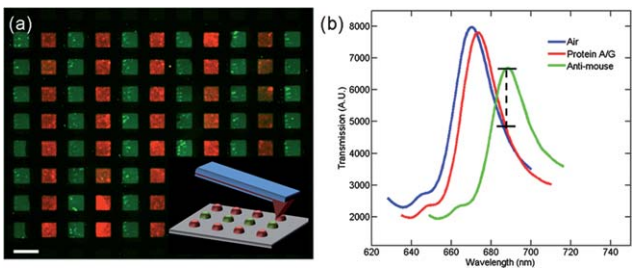

Fig. 4 Spectral response of microarray pixels spotted with bio-molecules. **(a)** Fluorescence image of different antibodies being immobilized on separate sensors show the multiplexing feature. The red areas are immobilized with anti-mouse IgG labeled with TRITC, and the green ones are anti-monkey labeled with FITC. Test bio-samples are spotted onto individual sensor elements by dip-pen spotting shown as inset. Scale bar, 30 μm. **(b)** Resonance of individual sensor pixel red-shifts after the immobilization of Protein A/G and anti-Mouse IgG. Transmission intensity reduces with accumulation of bio-molecules.

sensors are uniformly covered. Although the employed dip-pen lithography is suitable to demonstrate the multiplexing capability of the platform, it is a relatively slow technique due to its serial nature. For large-area microarray applications where large varieties of antibodies/proteins are needed to be immobilized rapidly, other surface spotting technologies can be also used.[38]

Label-free sensing of the analytes can be achieved by measuring the transmission spectrum and monitoring the EOT spectral shift of a sensing pixel. Spectral measurements are obtained sequentially following the protein A/G and goat anti-mouse IgG capturing. In Fig. 4b, the original resonance peak occurs at 670 nm (blue line). As molecules accumulate on the microarray surface, the (1,0) Au-Air resonance peak (red and green lines) red-shifts due to the increasing effective refractive index at the Au/air interface of the gold nanohole arrays. Attachment of 1 mg ml^{-1} protein A/G and 1 mg ml^{-1} goat anti-mouse IgG results in red shifts about 4 nm and 14 nm, respectively. The magnitude of the resonance shift with respect to bare surface allows direct quantification of the antibody molecules captured on the sensor surface. However, such measurements performed using a spectrometer is not suitable for high-throughput microarray applications since the sensors in the array needs to be evaluated sequentially rather than simultaneously. Therefore, alternative methods are needed for large-scale and massively multiplexed label-free detection.

Dual-color filter imaging method

For multiplexed detection, spectral shifts can be obtained from the variation of the spatial intensity distribution at a single wavelength captured as an image by a CCD camera.[35] For example, for the data presented in Fig. 4b, the initial resonance is

at 670 nm, and it red-shifts to 683 nm after antibody binding. This spectral shift can be detected by monitoring the intensity change at 695 nm (indicated by dashed line in Fig. 4b). However, with biomolecular accumulation, not only the resonance wavelength shifts, but also the transmission intensity drops as a result of increased absorption (as observed in Fig. 4b and our experimental measurements). This introduces reliability issues for quantitative analysis. To overcome this limitation, we developed a dual-color filter imaging method based on spectral ratio, which can significantly increase SNR. To investigate the limits of the method, we numerically calculated the expected signal using Matlab (given in Fig. 5a and 5b). Assume that the original resonance centers at 670 nm (blue curve in Fig. 5a). When the bio-molecules are captured, the resonance red-shifts to a higher wavelength with reduced intensity (red curve in Fig. 5a). There

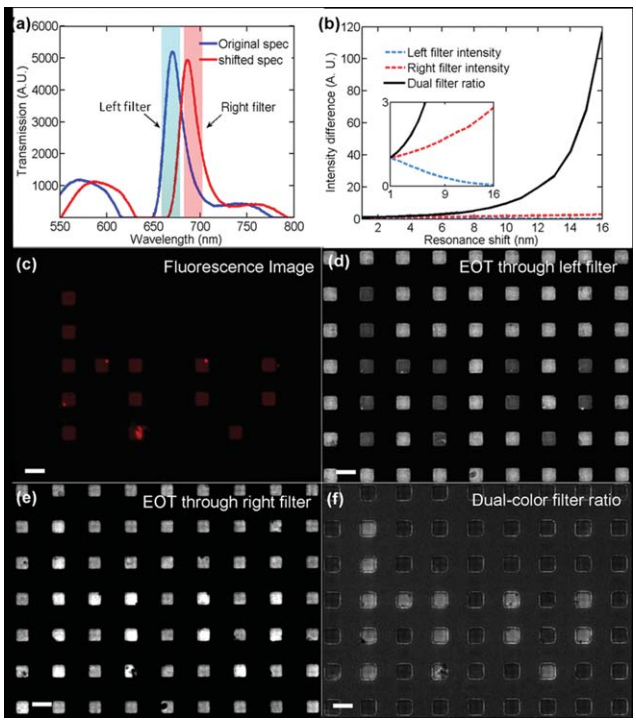

Fig. 5 Dual-color filter imaging method for label-free detection. (a)-(b) show simulation results. (c)-(f) show experimentally obtained images. (a) The original spectrum (blue) and the shifted one (red) are shown. Two optical filters, centered at 670 nm (light blue) and 695 nm (light red) are used to collect the transmission signals, respectively. (b) Normalized transmission intensity through the left filter as a function of resonance shift is shown in dashed blue line. Light intensity decreases due to the decreasing overlap between the filter and resonance peak. Dashed red line shows the transmission intensity through the right filter. As the resonance red-shifts, the light intensity increases. Dual-color filter imaging method is implemented by taking the ratio between the transmitted images from these two filters, which dramatically increases the signal-to-noise ratio (black line). The inset shows the zoom-in plot. (c) Fluorescence image of the antibody spotted sensor pixels, defining a word "hv". (Exposure time: 3 s) (d) EOT image through the left filter. The control pixels appear brighter. (e) EOT image through the right filter. The light intensity appears to be higher from the spotted pixels due to the red-shift of the spectrum, as contrary to the left filter. (f) Image processed using DcFI method. The image contrast is dramatically enhanced compared to the single filter method. (Exposure time: 30 ms)

are two optical band-pass filters with 20 nm bandwidth. The left filter is centered at 670 nm and the right filter is at 695 nm. The light intensity transmitted through left filter as a function of the resonance shift is shown in Fig. 5b with the dashed blue line. As the resonance red-shifts, the light intensity decreases due to the decreasing overlap of the resonance peak with transmission window of the filter. However, this single color filtering scheme, which measures intensity change at a single spectral window does not allow high signal-to-noise-ratio measurements. This shortcoming is demonstrated in experimental measurements as follows. After the microarray chip is functionalized with protein A/G, fluorescently labeled antibodies are captured at certain sensors defining a word "hv" as shown by fluorescence image in Fig. 5c. The rest of the sensing pixels in the array are used as controls. For incident light passing through the left filter, CCD images of the spatial intensity distribution are shown in Fig. 5d. Here, the transmitted light intensity obtained from the antibody captured sensors is not significantly weaker than those obtained from the control sensors. Similarly, numerical and experimental measurements using right filter gives signal with small SNR. For the right filter, the expected transmission intensity increases with the resonance shift (dashed red line in Fig. 5b). Experimental measurements confirm this result, and also show that the corresponding image has a small SNR and weak contrast. On the contrary, if we use DcFI method by taking the ratio between the transmitted signals from two filters, SNR is dramatically increased as illustrated in Fig. 5b and 5f. For instance, when the spectrum red-shifts by 14 nm after immobilization of 1 mg ml^{-1} anti-mouse IgG, the SNR of images acquired with our method is improved by 30 times compared to the single filter scheme. We should note that 20 nm bandwidth filter is used for the experimental implementation of our DcFI method. However, numerical calculation shows that the SNR can be further increased by using filters with narrower bandwidth. Fig. 5f experimentally demonstrates that the contrast of the image obtained by spectral ratio is better than the image obtained with single filter given in Fig. 5d and 5e. As a result, the patterned pixels forming the word "hv" is clearly observed. As shown in Fig. 5d and 5e, there are few sensing pixels with dark spots on them (*i.e.* on the sensor located in the last row of the fifth column) due to the defects introduced by fabrication imperfections. These pixels with low intensities may cause false positive/negative results in conventional label-free approaches. Notably, this effect can be removed effectively by our DcFI method (Fig. 5f).

To demonstrate quantitative measurement of molecular binding events, we used fluorescently-tagged anti-mouse IgG as analytes. After the microarray chip is functionalized with protein A/G, different concentration of analytes is spotted on specific sensor arrays. Their location is indicated in Fig. 6a by fluorescence measurements. Following incubation and subsequent washing, amount of accumulated analytes (*i.e* antibodies) at the corresponding sensors are measured using dual-color filter imaging technique. As shown in Fig. 6b, with increasing concentrations of analytes, stronger signals are obtained consistently by the DcFI method. Notably, the exposure time for the fluorescence signal was 3000 ms, but it took less than 30 ms for the EOT image. This corresponds to two orders of magnitude improvement in image acquisition time compared to the fluorescence methods.

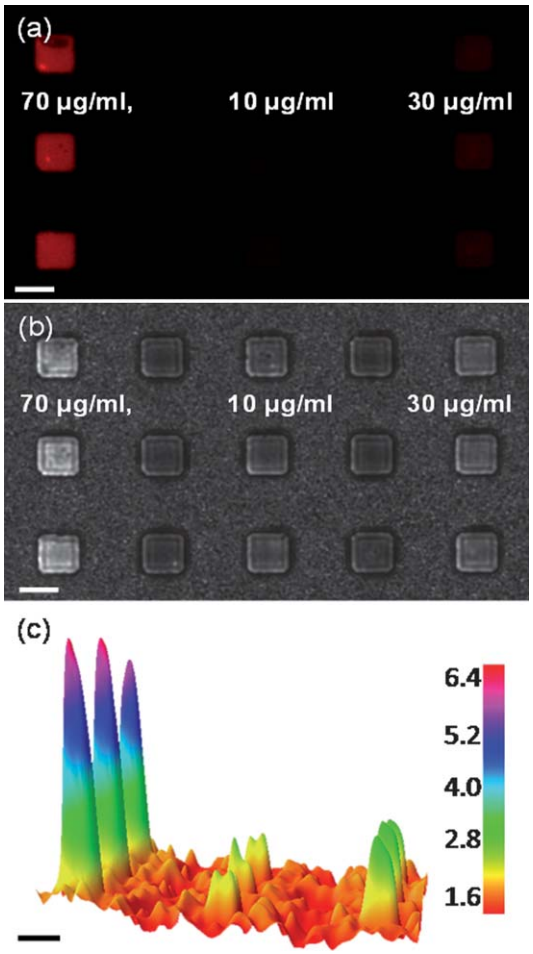

Fig. 6 Quantification of analyte concentration with label-free dual-color filter imaging method. **(a)** Fluorescence image of various concentrations of fluorescently labeled anti-mouse IgG used as analytes. Three different concentrations of 70 µl ml^{-1}, 10 µl ml^{-1} and 30 µl ml^{-1} analytes are shown respectively. **(b)** EOT image acquired by the DcFI method. **(c)** Dual-color filter image with different concentrations are shown in 3D for better visualization. Scale bar, 20 µm.

Discussion

Compared to conventional microarray technologies,[39] our large-area plasmonic microarrays can reliably enable quantitative and real-time detection in a label-free fashion. Obtaining the kinetic rates of biomolecular interactions in a high-throughput fashion (such as for determination of transcription factor binding sites, protein-small molecule bindings) can open up new opportunities in fundamental biology and pharmacology. On-chip configuration of the sensor can enable direct integration with microfluidics, which offers automated sample preparation and processing.[40–42] This platform can also be merged with recently emerging complementary technologies, such as lens-free on-chip microscopy and imaging,[43] and become widely applicable to various problems even in resources limited settings. Furthermore, compared to other nanobiosensors, our plasmonic platform using DcFI method is compatible with the existing infrastructure of conventional microarray spotters and scanners. This scheme can allow rapid implementation of the next generation of microarray technology with advanced capabilities and will become a powerful tool for biomedical sciences and pharmacology.

In conclusion, we present a label-free, high-throughput and low-cost plasmonic microarray technology. We introduced a dual-color filter imaging method, which increases the signal-to-noise of images more than 30 times compared to the detection method based on direct intensity change and enables to obtain images with large contrast. Using our method, reliable detection of biomolecular bindings is demonstrated. In addition, quantitative measurements of analyte binding events at a variety of concentrations are shown. Our platform also reduces the image acquisition time with respect to fluorescence technique by more than two orders of magnitude. To achieve large-area sensor arrays, we employed interference lithography which enabled uniform fabrication of sub-wavelength apertures over an entire microscope slide and resulted in more than a million sensors. The quality of sensors demonstrates high FOMs of 27 with refractive index sensitivity reaching to 615 nm/RIU. This label-free microarray technology, due to its ease of use, reliability and large-scale capability, can be a powerful tool for biomedical sciences and pharmacology.

Methods

Microarray fabrication

Fabrication scheme and setup are shown in Fig. 1a. The sample consists of a multi-layer stack on the front side of a microscope glass slide and a spin-coated thick layer of anti-reflection coating on the back side to eliminate reflection from the positioning stage. First, a 500 nm layer of Barli-ARC is spin-coated onto the back side of microscope slides and oven-baked at 175 °C. Sequentially, 200 nm of Poly(methyl methacrylate) (PMMA) and 220 nm of Barli-ARC is spin-coated onto the front side of the sample and oven-baked at 180 °C and 175 °C, respectively. After coating of 30 nm thick silicon oxide with an E-beam evaporator, a mono layer of hexamethyldisilazane (HMDS) is applied on top of the silicon oxide layer prior to spin-coating a 100 nm layer of positive-tone photoresist, Sumitomo PFI-88. The front side anti-reflection coating minimizes reflection from the bottom layer of the photoresist, HMDS coating enhances adhesion between the photoresist and silicon dioxide, and PMMA coating facilitates lift-off process. After sample preparation, a dual-exposure IL process, where each exposure takes 2 min, is applied on x and y axis for patterning the nanopillar square grid array in PFI-88. The interference lithography setup consists of a spatially-filtered He-Cd laser at 325 nm wavelength. After exposure, the sample is developed in CD-26 and 0.26% Tetramethylammonium hydroxide (TMAH) for 45 s. Following the interference lithography process and development, reactive ion etching (RIE) is applied with CF_4 and He/O_2 for transferring the pattern into SiO_x and the underlying ARC/PMMA layer. Lastly, 100 nm of gold is evaporated *via* E-beam evaporation and PMMA/gold patterned regions are lifted off in 60 °C acetone with ultrasonic agitation for 10 min. Using this process, we can easily and cost effectively pattern nanohole arrays on whole microscope slides or glass wafers within few minutes and finish the whole process within few hours. The microarray platform is divided by introducing Cr spacers between individual sensors using

photolithography and Cr deposition. Cr spacer blocks the light transmission and minimizes the SPR interaction between sensors by absorbing the propagating of SPR.

Protein spotting on microarray

For spotting, the gold surfaces are first functionalized with protein A/G at a concentration of 1 mg mL^{-1} diluted in PBS (10 mM phosphate buffer, 137 mM NaCl, and 2.7 mL of KCl). Protein A/G is chosen as a template for the immobilization of the antibodies due to its high affinity to the Fc region of the IgG molecules.[44] Two different antibodies labeled with different fluorophores, anti-mouse IgG from goat (labeled with TRITC) and anti-monkey from rabbit (labeled with FITC), are spotted onto the sensing sensors. The concentrations of both antibodies are 1mg ml^{-1} diluted in a PBS-glycerol mixture. Glycerol is used to keep the solution from drying during the spotting, and also helps to keep the spotted droplets uniform. The 30 μm AFM tip yields a round droplet with diameter of 30–35 μm at a specific humidity and AFM tapping force. After 30 min of incubation, unbound antibodies are removed by a three-step PBS washing process.

Acknowledgements

We thank P. Tillberg, J.A. Koo, M. Angel and B. Kim for their comments on the manuscript. This work was supported in part by National Science Foundation (NSF) CAREER Award (ECCS-0954790), Office of Naval Research Young Investigator Award, Massachusetts Life Science Center New Investigator Award, NSF Engineering Research Center on Smart Lighting (EEC-0812056), Boston University Photonics Center. T.Y.C was supported by the Foxconn sponsorship and M.H. was supported by NSF.

Author contributions

T.Y.C., M.H., H.Y.T, P.S. and H.A designed experiments; T.Y.C., M.H., A.A.Y., M.F.Y. and H.A wrote the manuscript; T.Y.C., M.H. and H.Y.T performed the experiments.

References

1 J. Ziauddin and D. M. Sabatini, Microarrays of cells expressing defined cDNAs, *Nature*, 2001, **411**, 107–110.
2 L. P. Lim, *et al.* Microarray analysis shows that some microRNAs downregulate large numbers of target mRNAs, *Nature*, 2005, **433**, 769–773.
3 G. MacBeath and S. L. Schreiber, Printing proteins as microarrays for high-hroughput function determination, *Science*, 2000, **289**(No. 5484), 1760–1763.
4 A. Sassolas, B. D. Leca-Bouvier and L. J. Blum, DNA biosensors and microarrays, *Chem. Rev.*, 2008, **108**, 109–139.
5 L. Zhang, T. Hurek and B. Reinhold-Hurek, Position of the fluorescent label is a crucial factor determining signal intensity in microarray hybridizations, *Nucleic Acids Res.*, 2005, **33**, e166.
6 U. Resch-Genger, M. Grabolle, S. Cavaliere-Jaricot, R. Nitschke and T. Nann, Quantum dots *versus* organic dyes as fluorescent labels, *Nat. Methods*, 2008, **5**, 763–775.
7 H. J. Gruber, *et al.* Anomalous fluorescence enhancement of Cy3 and Cy3.5 *versus* anomalous fluorescence loss of Cy5 and Cy7 upon covalently linking to IgC and noncovalent binding to avidin, *Bioconjugate Chem.*, 2000, **11**, 696–704.
8 Y. Cui, Q. Q. Wei, H. K. Park and C. M. Lieber, Nanowire nanosensors for highly sensitive and selective detection of biological and chemical species, *Science*, 2001, **293**, 1289–1292.
9 Y. L. Bunimovich, *et al.* Quantitative real-Time measurements of DNA hybridization with alkylated nonoxidized silicon nanowires in electrolyte solution, *J. Am. Chem. Soc.*, 2006, **128**, 16323–16331.
10 J. Lee, J. Jang, D. Akin, C. A. Savran and R. Bashir, Real-time detection of airborne viruses on a mass-sensitive device, *Appl. Phys. Lett.*, 2008, **93**, 013901.
11 J. Fritz, *et al.* Translating biomolecular recognition into nanomechanics, *Science*, 2000, **288**, 316–318.
12 C. A. Savran, S. M. Knudsen, A. D. Ellington and S. R. Manalis, Micromechanical detection of proteins using aptamer-based receptor molecules, *Anal. Chem.*, 2004, **76**, 3194–3198.
13 X. Fan, *et al.* Sensitive optical biosensors for unlabeled targets: A review, *Anal. Chim. Acta*, 2008, **620**, 8–26.
14 J. Homola, Present and future of surface plasmon resonance biosensors, *Anal. Bioanal. Chem.*, 2003, **377**, 528–539.
15 S. Se, *et al.* High-throughput lens-free blood analysis on a chip, *Anal. Chem.*, 2010, **82**, 4621–4627.
16 E. Cubukcu, *et al.* Aligned carbon nanotubes as polarization-sensitive molecular near-field detectors, *Proc. Natl. Acad. Sci. U. S. A.*, 2009, **106**, 2495–2499.
17 M. I. Rudenko, *et al.* Ultrasensitive Q [beta] phage analysis using fluorescence correlation spectroscopy on an optofluidic chip, *Biosens. Bioelectron.*, 2009, **24**, 3258–3263.
18 J. Lee, K. Icoz, A. Roberts, A. D. Ellington and C. A. Savran, Diffractometric detection of proteins using microbead-based rolling circle amplification, *Anal. Chem.*, 2010, **82**, 197–202.
19 A. Kinkhabwala, Z. Yu, S. Fan, Y. Avlasevich, K. Müllen and W. E. Moerner, Large single-molecule fluorescence enhancements produced by a bowtie nanoantenna, *Nat. Photonics*, 2009, **3**, 654–657.
20 M. A. Cooper, Optical biosensor in drug discovery, *Nat. Rev. Drug Discovery*, 2002, **1**, 515.
21 J. Homola, H. Vaisocherova, J. Dostalek and M. Piliarik, Multi-analyte surface plasmon resonance biosensing, *Methods*, 2005, **37**, 26–36.
22 A. A. Yanik, M. Huang, A. Artar, T. Y. Chang and H. Altug, Integrated nanoplasmonic-nanofluidic biosensors with targeted delivery of analytes, *Appl. Phys. Lett.*, 2010, **96**, 021101.
23 A. A. Yanik, *et al.* An optofluidic nanoplasmonic biosensor for direct detectionof live viruses from biological media, *Nano Lett.*, 2010, **10** (12), 4962–4969.
24 B. Khademhosseini, *et al.* Lensfree densing on a micro-fluidic chip using plasmonic nano-apertures, *Appl. Phys. Lett.*, 2010, **97**, 221107.
25 K. A. Tetz, L. Pang and Y. Fainman, High-resolution surface plasmon resonance sensor based on linewidth-optimized nanohole array transmittance, *Opt. Lett.*, 2006, **31**, 1528–1530.
26 N. Liu, *et al.* Planar Metamaterial Analogue of electromagnetically induced transparency for plasmonic sensing, *Nano Lett.*, 2010, **10** (4), 1103–1107.
27 T. W. Ebbesen, H. J. Lezec, H. F. Ghaemi, T. Thio and P. A. Wolff, Extraordinary optical transmission through sub-wavelength hole arrays, *Nature*, 1998, **391**, 667–669.
28 W. L. Barnes, A. Dereux and T. W. Ebbesen, Surface plasmon subwavelength optics, *Nature*, 2003, **424**, 824–830.
29 A. O. Cakmak, *et al.* Enhanced transmission through a subwavelength aperture using metamaterials, *Appl. Phys. Lett.*, 2009, **95**, 052103.
30 A. B. Khanikaev, S. H. Mousavi, G. Shvets and Y. S. Kivshar, One-Way Extraordinary Optical Transmission and Nonreciprocal Spoof Plasmons, *Phys. Rev. Lett.*, 2010, **105**, 126804.
31 A. De Leebeeck, *et al.* On-chip surface-based detection with nanohole arrays, *Anal. Chem.*, 2007, **79**, 4094–4100.
32 F. Eftekhari, *et al.* Nanoholes as nanochannels: flow-through plasmonic sensing, *Anal. Chem.*, 2009, **81**(11), 4308–431.
33 M. R. Lee and P. M. Fauchet, Two-dimensional silicon photonic crystal based biosensing platform for protein detection, *Opt. Express*, 2007, **15**, 4530–4535.
34 H. Altug and J. Vuckovic, Polarization control and sensing with two-dimensional coupled photonic crystal microcavity arrays, *Opt. Lett.*, 2005, **30**, 982–984.
35 J. Zhu, *et al.* On-chip single nanoparticle detection and sizing by mode splitting in an ultrahigh-Q microresonator, *Nat. Photonics*, 2010, **4**, 46–49.
36 J. Ji, G. Connell, D. J. D. Carter and D. N. Larson, High-throughput nanohole array based system to monitor multiple binding events in real time, *Anal. Chem.*, 2008, **80**, 2491–2498.

37 J. Henzie, M. H. Lee and T. W. Odom, Multiscale patterning of plasmonic metamaterials, *Nat. Nanotechnol.*, 2007, **2**, 549–554.
38 M. Dufva, Fabrication of high quality microarrays, *Biomol. Eng.*, 2005, **22**, 173–184.
39 S. Choudhuri, Microarrays in biology and medicine, *J. Biochem. Mol. Toxicol.*, 2004, **18**, 171–179.
40 S. Nagrath, *et al.* Isolation of rare circulating tumor cells in cancer patients by microchip technology, *Nature*, 2007, **450**, 1235–1239.
41 C. Pardo-Martin, *et al.* High-throughput in vivo vertebrate screening, *Nat. Methods*, 2010, **7**, 634–636.
42 C. B. Rohde, F. Zeng, R. Gonzalez-Rubio, M. Angel and M. F. Yanik, Microfluidic system for on-chip high-throughput whole-animal sorting and screening at subcellular resolution, *Proc. Natl. Acad. Sci. U. S. A.*, 2007, **104**, 13891–13895.
43 S. Seo, T. W. Su, D. K. Tseng, A. Erlinger and A. Ozcan, Lensfree holographic imaging for on-chip cytometry and diagnostics, *Lab Chip*, 2009, **9**, 777–787.
44 S. R. Nettikadan, J. C. Johnson, S. G. Vengasandra, J. Muys and E. Henderson, ViriChip: a solid phase assay for detection and identification of viruses by atomic force microscopy, *Nanotechnology*, 2004, **15**, 383.

